Synchronization Conditions and Desynchronizing Patterns in Coupled Limit-Cycle and Chaotic Systems

Louis M. Pecora

Code 6343

Naval Research Laboratory

Washington, DC 20375

Abstract. Many coupling schemes for both limit-cycle and chaotic systems involve adding linear combinations of dynamical variables from various oscillators in an array of identical oscillators to each oscillator node of the array. Examples of such couplings are (nearest neighbor) diffusive coupling, all-to-all coupling, star coupling, and random linear couplings. We show that for a given oscillator type and a given choice of oscillator variables to use in the coupling arrangement, the stability of each linear coupling scheme can be calculated from the stability of any other for symmetric coupling schemes. In particular, when there are desynchronization bifurcations our approach reveals interesting patterns and relations between desynchronous modes, including the situation in which for some systems there is a limit on the number of oscillators that can be coupled and still retain synchronous chaotic behavior.

PACS NO. 05.45.+b, 47.20 Ky, 84.30. -r

To appear in Physical Review E

I. Introduction

The phenomenon of synchronization of identical chaotic systems coupled in an array has recently received a great deal of attention [1-18] although the behavior was shown to exist some years ago [19-22]. Similarly, the synchronization of coupled limit cycle systems continues to be of great interest (see Refs. [23-29] for a sampling of this large field). For chaotic systems one's intuition about synchronization criteria and conditions can fail. There is no sharp synchronization threshold. Instead there are multiple thresholds, each associated with an unstable period orbit (UPO) [6, 30-32]. There may be riddled basins [8, 33-35] so that predicting the synchronized state is nearly impossible by just knowing initial conditions. Above the Lyapunov exponent synchronization threshold there can be intermittent bursting (often called *attractor bubbling*) of the systems out of the synchronous state when there is a small amount of noise or parameter mismatch present [6, 30-32].

There are even desynchronization bifurcations in which increasing the coupling between systems in the coupled array may *destabilize* the synchronous state. This latter phenomenon was also called a *short-wavelength bifurcation* [36]. These unexpected behaviors are documented in real physical systems in Refs. [8, 10, 12, 36]. A few other researchers have also seen such bifurcations [37, 38] in phase-locked loops and Josephson junctions.

We note that when we use the term desynchronization bifurcation here we mean that the system has qualitatively changed because the synchronous state is no longer stable. We are not in a position to discuss, in general, what new state, if any, will result, only that it will not be the synchronous one. However, we will see below that we can describe the initial pattern of desynchronization.

The phenomenon of short-wavelength bifurcation (SWB) is very intriguing. It is a desynchronizing bifurcation that sometimes occurs in diffusively-coupled, arrays of oscillators and is caused by increasing the coupling. When it occurs in these arrays it means that the

shortest spatial wavelength (in the sense of a discrete space) in the system is excited to cause the systems to desynchronize. Such a bifurcation beginning at extremely small spatial lengths has also been referred to as a *spatio-temporal shredding bifurcation* [39] for obvious reasons. Direct evidence for this phenomenon in limit cycle systems was shown in Watanabe *et al*. [37] where they show basic instabilities seen in Josephson junction systems result from short-wavelength bifurcations. Goldstein and Strogatz also showed that such bifurcations can occur in phase-locked loops.

Short-wavelength bifurcations in chaotic arrays further implie that there is an upper limit (a size limit) to the number of chaotic nodes that can be added to the array while keeping the synchronized state stable. Heagy *et al*. [36] show that this maximum number can be calculated if one knows the stability diagram.

We show here that a similar desynchronization bifurcation can take place in a coupled array of limit cycle oscillators. Again, increasing the coupling in these circumstances can cause the counter-intuitive desynchronization to take place. We show that similar stability analyses can be used for both chaotic and limit cycle oscillator arrays to understand the pattern that first emerges in this bifurcation. This leads to analysis of a canonical variational equation which holds for a large number of coupled array systems. In fact, for many coupled arrays with various symmetric couplings we can show that some type of SWB is possible for many systems and for chaotic, coupled systems this will necessarily mean a size limit on a synchronized array.

Recently Wu and Chua [40] conjectured that there was a relationship between the coupling constants and the eigenvalues of coupling matrices in linearly coupled arrays of oscillators. The conjecture is, if an array with m_1 number of oscillators synchronizes at a coupling constant = α_1, then another similarly-coupled array of size m_2 will synchronize at a coupling constant = α_2 such that the following relation is preserved

$$\alpha_1 \mu_1 = \alpha_2 \mu_2 , \qquad (1)$$

where μ_1 and μ_2 are the eigenvalues of the coupling matrices for the m_1 and m_2 array, respectively.

We show that in light of the SWB and size limits in chaotic arrays this conjecture must be false in general. We develop exact relations between the coupling constants and the coupling eigenvalues for different sized arrays with various linear couplings that can be used to predict the stability of desynchronizing spatial *modes*. We show that the Wu and Chua relation (Eq. (1)) really reflects the stability of individual modes, but not necessarily the stability of the entire system. We explain this in more detail below.

II. Motivating Example: Limit Cycle Rössler Array

A. System configuration

We start off with a motivating limit cycle example. The example contains many of the features that will emerge in a general analysis that we undertake later in this paper.

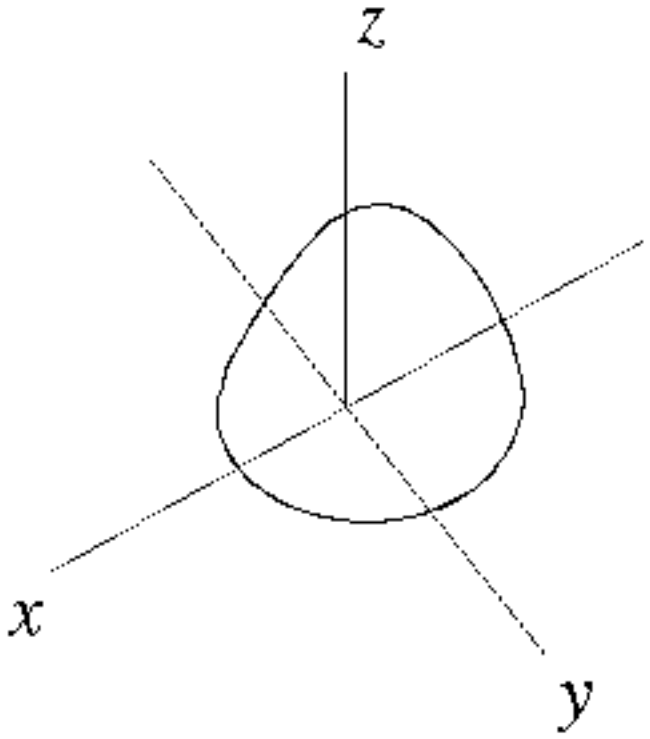

Fig. 1 Rössler limit-cycle attractor.

The Rössler system [41] (Eq. (2)) is well-known for its chaotic behavior. It also has simple, limit cycle behavior. For the parameters a=0.2, b=0.2, c=2.5 the system has one attractor which is a simple, period-1 limit cycle (see Fig. 1).

$$\begin{aligned} \frac{dx}{dt} &= -(y+z) \\ \frac{dy}{dt} &= x + ay \\ \frac{dz}{dt} &= b + z(x-c) \end{aligned} \quad . \qquad (2)$$

We link *n* of these attractors in a circle with nearest-neighbor or diffusive coupling (DC):

$$\begin{aligned} \frac{dx_i}{dt} &= -(y_i + z_i) + \alpha\varepsilon_{xx}(x_{i+1} + x_{i-1} - 2x_i) \\ \frac{dy_i}{dt} &= x_i + ay_i + \alpha\varepsilon_{yy}(y_{i+1} + y_{i-1} - 2y_i) \\ \frac{dz_i}{dt} &= b + z_i(x_i - c) \end{aligned} \quad , \qquad (3)$$

where we have the option to couple through either the *x* component (using ε_{xx}=1 and ε_{yy}=0) or the *y* component (using ε_{xx}=0 and ε_{yy}=1). Obviously, other combinations and weightings are possible, but we want to keep things simple enough to analyze. Generalizations will be obvious later.

B. Stability of the synchronous state

We want to examine the stability of the synchronous state in which all oscillators are behaving as in Fig. 1 as a function of the coupling parameter α . The tools to do this for diffusive coupling were developed in an earlier paper [3] and we outline the scheme here.

The geometry of the synchronous attractor is such that it lies on a hyperplane determined by the *n*-1 vector equalities

$$(x_1, y_1, z_1) = (x_2, y_2, z_2) = \ldots = (x_n, y_n, z_n) . \qquad (4)$$

The hyperplane is called the *synchronization manifold* and has dimension=3. This is shown schematically in Fig. 2; all the node lines (x_1=x_2, etc.) are in the synchronization manifold. As long as the entire system's phase space point remains on the synchronization manifold the systems remain in sync. Thus, for stability we need to have *all* motion transverse to the manifold damped out. The Lyapunov exponents (or Floquet multipliers for the limit cycle cases) for

transverse motion will indicate when this will happen. This means we need to study the variational equation which will lead us to examine the Jacobian for the array.

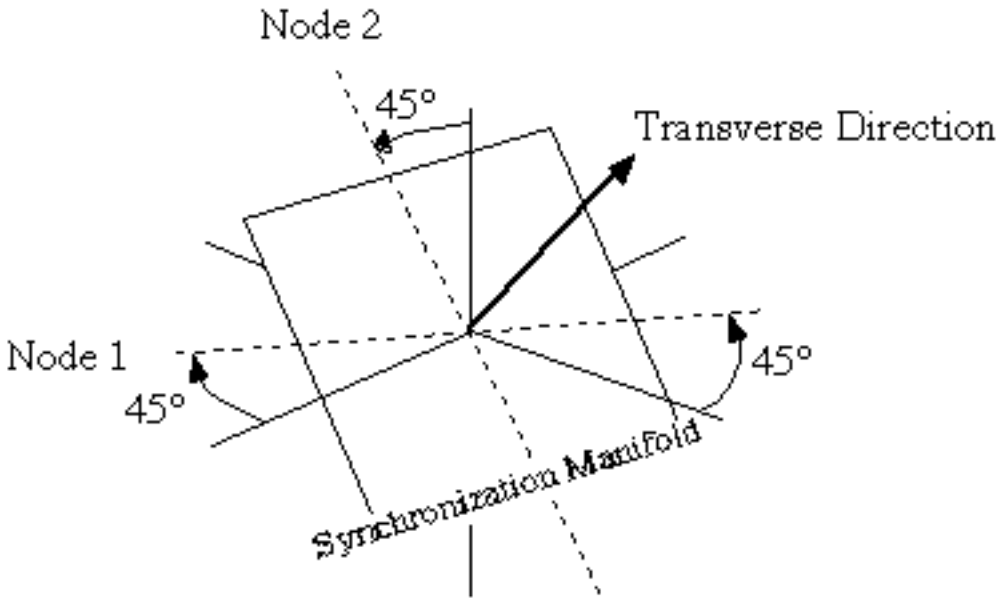

Fig. 2 Schematic geometry of the synchronization manifold which lies along the "45°" lines between all coordinates. Orthogonal (transverse) to the synchronization manifold are coordinates that represent non-synchronous behavior.

The Jacobian for the whole system has the following structure:

$$\begin{pmatrix} \mathbf{J}-2\alpha\mathbf{E} & \alpha\mathbf{E} & 0 & 0 & \dots & \alpha\mathbf{E} \\ \alpha\mathbf{E} & \mathbf{J}-2\alpha\mathbf{E} & \alpha\mathbf{E} & 0 & \dots & 0 \\ 0 & \alpha\mathbf{E} & \mathbf{J}-2\alpha\mathbf{E} & \alpha\mathbf{E} & \dots & 0 \\ \vdots & \vdots & \vdots & \vdots & \dots & \vdots \\ \alpha\mathbf{E} & 0 & 0 & \dots & \alpha\mathbf{E} & \mathbf{J}-2\alpha\mathbf{E} \end{pmatrix}, \tag{5}$$

where **J** is the Jacobian of a single (synchronized, uncoupled) Rössler,

$$\mathbf{J} = \begin{pmatrix} 0 & -1 & -1 \\ 1 & a & 0 \\ z & 0 & x-c \end{pmatrix} \tag{6}$$

and **E** is the coupling matrix,

$$\mathbf{E} = \begin{pmatrix} \varepsilon_{xx} & 0 & 0 \\ 0 & \varepsilon_{yy} & 0 \\ 0 & 0 & 0 \end{pmatrix}. \qquad (7)$$

In order to deal with the Jacobian in (5) we treat each block as though it were a single entry in a matrix. This is a direct product structure which we will show explicitly in later sections and the appendix.

What we would like to do is diagonalize (5) in a coordinate system that isolates the stability of the synchronization manifold from the transverse directions. The synchronization manifold can be thought of as lying along the "major diagonal" in the block structure space of Eq. (5): (**1**,**1**,**1**,...**1**), where **1**=(1,1,1). This direction is defined by the vector $\mathbf{f}=\mathbf{e}_1+\mathbf{e}_2+...+\mathbf{e}_n$, where $\mathbf{e}_i$ is the unit vector in the *i*th block. Thus, if we can find coordinates orthogonal to **f** and if they diagonalize (5) we can analyze the stability.

Eq. (5) has a cyclic block structure [42], also known in the solid state field as nearest neighbor coupling with periodic boundary conditions [43-45] and in the dynamics field as shift-invariant systems [46, 47]. It is well known that one can use discrete Fourier transformations to block diagonalize such systems. In Ref. [3] we showed that indeed this could be done for chaotic, synchronized systems. It can just as easily be done for limit cycle systems or any systems which are all behaving identically.

To transform to the Fourier basis we define new block bases vectors:

$$\begin{aligned} \mathbf{f}_0 &= \frac{1}{n}\sum_{j=1}^{n} \mathbf{e}_j \\ \mathbf{f}_k &= \frac{1}{n}\sum_{j=1}^{n} \mathbf{e}_j \; e^{2\pi i jk/n} \end{aligned}, \qquad (8)$$

where *k* runs from 0 to *n*-1 (we show the *k*=0 case separately for clarity). We see that $\mathbf{f}_0$ is just our synchronization manifold and from the orthogonality of Fourier series we have that the $\mathbf{f}_k$ ($k\neq 0$) are orthogonal to the synchronization manifold. This change of coordinates gives a Jacobian

$$\begin{pmatrix} \mathbf{J} & 0 & 0 & 0 & \dots & 0 \\ 0 & \mathbf{J}+\alpha\mathbf{E}\gamma_1 & 0 & 0 & \dots & 0 \\ 0 & 0 & \mathbf{J}+\alpha\mathbf{E}\gamma_2 & 0 & \dots & 0 \\ 0 & 0 & 0 & \mathbf{J}+\alpha\mathbf{E}\gamma_3 & \dots & 0 \\ \vdots & \vdots & \vdots & \vdots & \vdots & \vdots \\ 0 & 0 & 0 & 0 & \dots & \mathbf{J}+\alpha\mathbf{E}\gamma_{n-1} \end{pmatrix}, \tag{9}$$

where

$$\gamma_k = -4\sin^2(\pi k/n). \tag{10}$$

We note that because of the shift-invariant symmetry $\gamma_k=\gamma_{n-k}$. The highest spatial-frequency mode corresponds to k=[[n/2]] ([[.]] means integer part of) and this is associated with the shortest wavelength of the discrete space. Because of the symmetry we need only examine the stability of the modes for k=0 to [[n/2]].

We have reduced the problem to one of finding the stability given by the individual block variational equations:

$$\frac{d\xi_k}{dt} = (\mathbf{J}+\alpha\mathbf{E}\gamma_k)\xi_k, \tag{11}$$

wshere ξ_k represents a perturbation of the kth mode. This form of variational equation shows up in many problems of stability of driven and/or coupled systems [3, 11, 12, 14, 19, 36, 40, 47-51] as well as in control theory methods [9, 52-58]. It is often not solvable since, although $\alpha\mathbf{E}\gamma_k$ is constant, **J** is not. However, we can use various scaling relations along with numerical solutions to understand the overall stability of the synchronized system as given by Eq. (9).

Each block in Eq. (9) corresponds to a spatial Fourier mode. The k=0 mode describes the motion restricted to the synchronization manifold and its Lyapunov exponents are those of the isolated dynamical unit. All other ($k \neq 0$) modes describe the system's response to small deviations from the synchronization manifold. We want to find out if *all* of these fluctuations damp out. Only then will the synchronous state be stable. As we noted previously [3, 10, 36], finding the stability of all the modes is actually not as arduous a task as it might seem. The following scaling relation holds

$$\alpha E\gamma_k = \alpha E\left(\frac{\gamma_k}{\gamma_1}\right)\gamma_1, \qquad (12)$$

meaning that the variational equation for the *k*th mode has the same form as for the first mode with a modified coupling constant $\alpha\,(\gamma_k/\gamma_1)$. Hence, once we find the Lyapunov exponents for mode 1 as a function of coupling, we can rescale the relation and we automatically have the exponents for all other modes. Since we really only need look at whether the maximum exponent is negative or not, we examine only that one λ^{k}_{max} for each mode *k*.

C. A short-wavelength bifurcation

Continuing the analysis of our example, we calculate the dependence of the maximum exponent for mode 1 as a function of both coupling constants in *x* and *y* variables. Then we see what the scaling relations tell us about the stability of all the modes. Fig. 3 shows the stability diagram for an array of 6 Rössler systems using *x*-coupling (ε_{yy}=0). We started with the stability of mode 1 and used Eq. (12) to calculate the stability of modes 2 and 3. The γ_k factors are monotonically increasing with *k*. This causes each stabilty diagram for increasingly higher modes to be compressed more toward the origin (see Fig. 3).

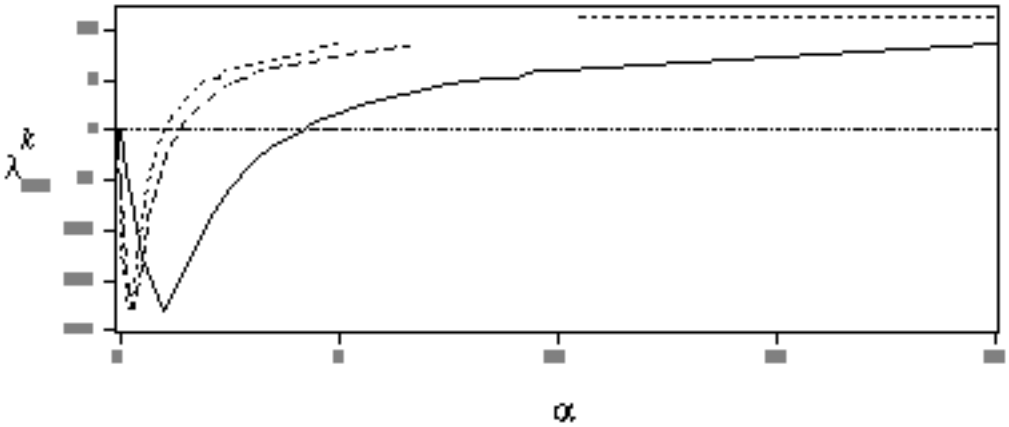

Fig. 3 Stability diagram for modes 1,2,3 of a 6 limit-cycle Rössler array with *x*-coupling. Solid line is mode 1, dotted line is mode 2, and dashed line is mode 3. The horizontal dashed line at large coupling values is the asymptotic limit at $c=\infty$ for λ^{k}_{max}.

We see that just above α=0 all modes are stable, hence this arrangement can support stable, synchronized limit cycle behavior. The values of λ_{max}^{k} start at 0 for α =0 since for uncoupled limit cycles the largest exponent is the neutral direction along the flow. As α increases all modes at first become more stable, but at larger values of α something more interesting happens. The stability trend reverses and the modes become less stable. Eventually, all modes become unstable and the synchronous state likewise becomes unstable. We refer to such changes in stability with changes in coupling as *desynchronizing bifurcations*.

The desynchronizing bifurcation takes place in an interesting way. Typically in DC systems the longest wavelength mode (mode 1) is the last to become stable as the coupling increases and the shortest wavelength mode (mode 3, here) is the most stable. However, when there is a desynchronizing bifurcation with increasing coupling the situation is reversed. It is the shortest wavelength that becomes unstable first as coupling increases. Thus, it is the shortest wavelength that first destabilizes the synchronous state. In a synchronized, DC, chaotic system we have a similar phenomenon which we called a *short-wavelength bifurcation* (SWB) [36]. When there is an obvious wavelength we will often refer to these desynchronizing bifurcations as SWB, although, as we will see below, some coupling schemes do not allow a straight-forward wavelength interpretation.

We can understand why the system eventually has to destabilize by studying the coupling in an asymptotic regime, namely at infinite coupling (α =∞). In this regime the coupling terms in Eqs. (3) dominate the other terms and cause the *x*-components to become slaved to each other and to the synchronous state. Thus, the remaining dynamical variables in each oscillator which are not coupled to other oscillators act like a driven system with $x(t)$ as the drive and the problem of stability is reduced to studying the stability of the subsystem ($\dot{y}$, $\dot{z}$). This is exactly the case we originally studied in synchronization of chaotically driven systems [59-62]. In fact it is easy to see from the Jacobian of the (y, z) subsystem that this subsystem must be unstable. Hence at large coupling values the stability of the modes must approach the stability of the subsystem, which is unstable in this case. We see this happening in Fig. 3.

The interesting observation here is that it is an *increase* in coupling that causes the modes to become unstable. Although this is counter-intuitive, it has been known in a different form before from the work of Turing [63] where it was used to describe the occurrence of patterns with intermediate wavelengths. In our present case the SWB is an extreme form of a Turing bifurcation. Turing kept some coupling between all the dynamical variables whereas we have in each oscillator a subsystem (e.g. the *y*-*z* system for *x* coupling) whose variables are *not* directly coupled to any other oscillator. Thus, in our case it is the absolute shortest wavelength in the system which becomes unstable first not the intermediate wavelengths. A plot of the entire system in Fig. 4 shows the effects of this desynchronizing bifurcation on the spatio-temporal

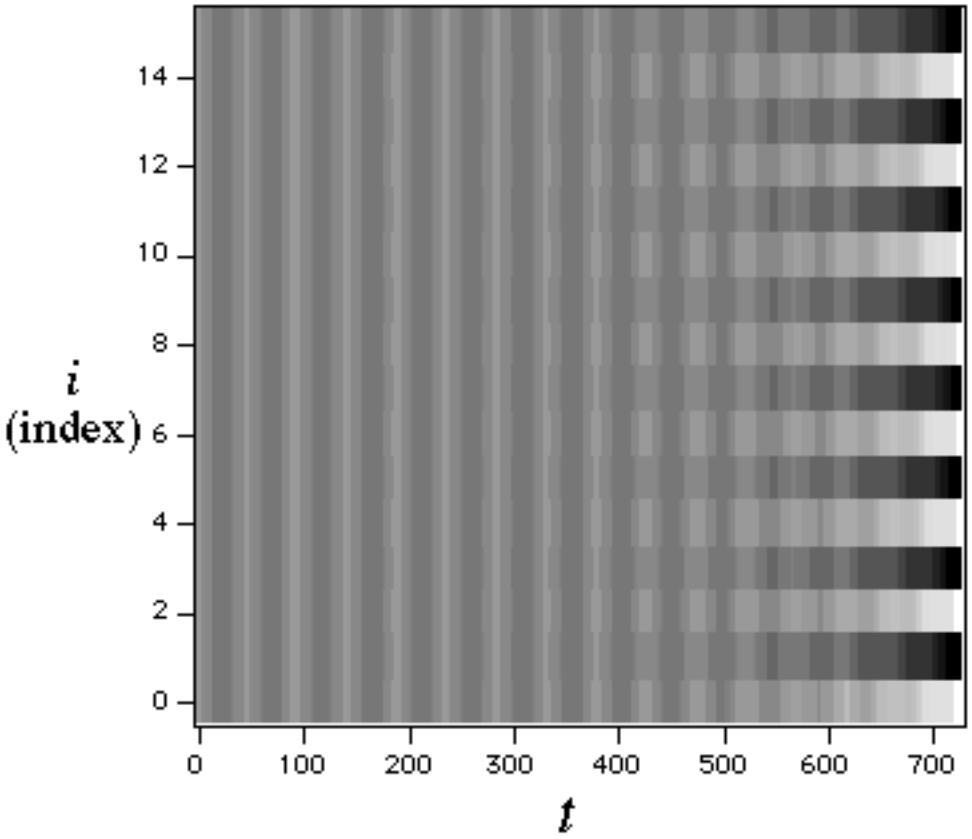

Fig. 4 Spatiotemporal pattern showing the onset of a short-wavelength bifurcation in an array of 16, *x*-coupled Rössler oscillators.

pattern of behavior. The desynchronization occurs with the dynamical variables of adjacent oscillators diverging in opposite directions in phase space, a manifestation of the short-wavelength instability. We also refer to this type of instability as *spatio-temporal shredding*, for obvious reasons.

In Fig. 5 we show a stability diagram for *y* coupling (ε_{xx}=0, ε_{xx}=1). We see that this coupling of Rössler limit cycle oscillators also gives rise to a SWB. The asymptotic value of λ^{k}_{max} is not as large for *y* coupling as for *x* coupling. As a result the desynchronization bifurcation takes place at larger coupling values.

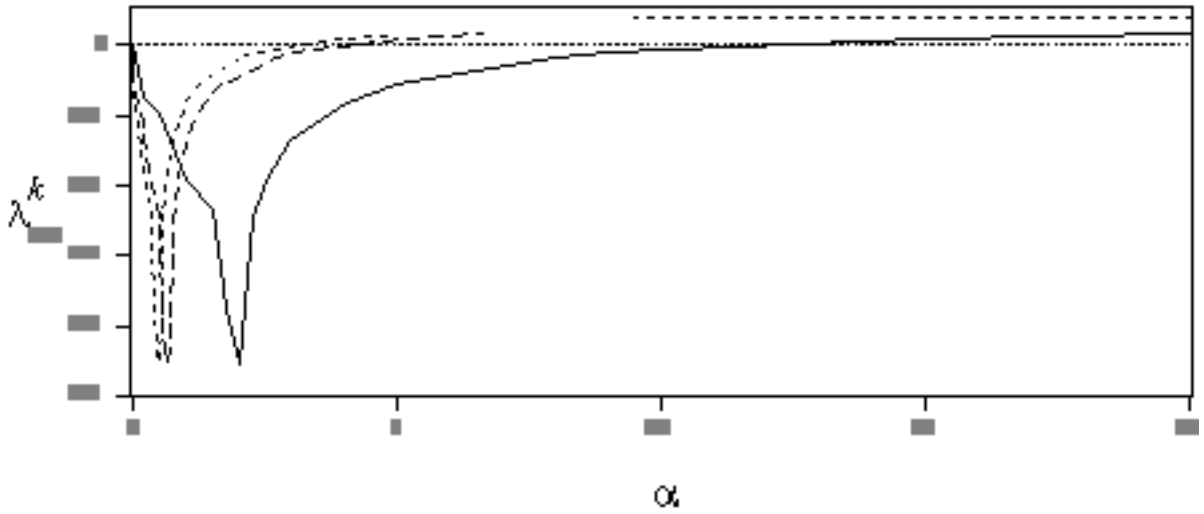

Fig. 5 Stability diagram for modes 1,2,3 of a 6 limit-cycle Rössler array with *y*-coupling. Solid line is mode 1, dotted line is mode 2, and dashed line is mode 3. The horizontal dashed line at large coupling values is the asymptotic limit at $c=\infty$ for λ^{k}_{max}.

As an interesting comparison we examine the synchronization of DC chaotic Rössler oscillators (c=7.0). The above stability analysis carries through regardless of the type of oscillator dynamics and we end up with the same variational equation (Eq. (11)) and scaling relation (Eq. (12)). Fig. 6 shows the stability diagram for *x* coupling. We see a diagram similar to Fig. 3, except that λ^{k}_{max} starts at a positive value when α =0, since the uncoupled systems are chaotic. The value of λ^{k}_{max} decreases from there as α increases and then increases to cause a SWB as in the limit cycle regime. Fig. 7 shows the stability diagram for *y* coupling. In this case

there is no SWB. Even for infinite coupling λ^{k}_{max} is negative and so the synchronized, chaotic stat

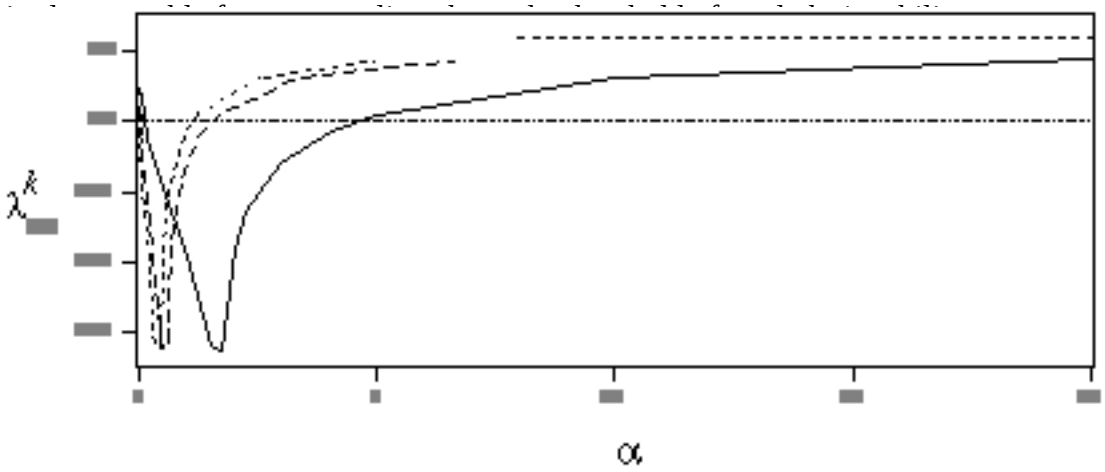

Fig. 6 Stability diagram for modes 1,2,3 of a 6 chaotic Rössler array with *x*-coupling. Solid line is mode 1, dotted line is mode 2, and dashed line is mode 3. The horizontal dashed line at large coupling values is the asymptotic limit at $c=\infty$ for λ^{k}_{max}.

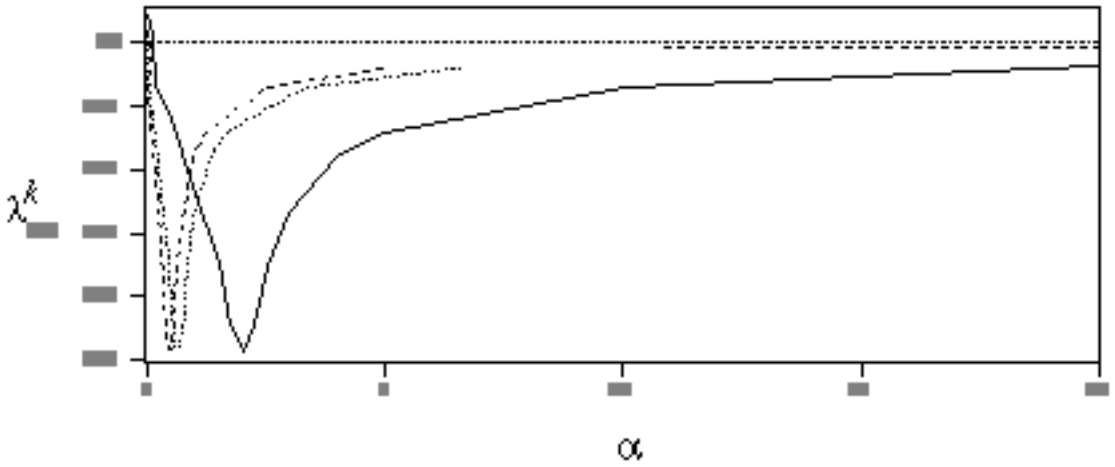

Fig. 7 Stability diagram for modes 1,2,3 of a 6 chaotic Rössler array with *y*-coupling. Solid line is mode 1, dotted line is mode 2, and dashed line is mode 3. The horizontal dashed line at large coupling values is the asymptotic limit at $c=\infty$ for λ^{k}_{max}.

D. Size limits on synchronizable systems resulting from short-wavelength bifurcations

In the chaotic case there is an effect that results from the SWB which is not present in the limit cycle case. Fig. 8 Shows a close up of part of the stability diagram for 20 chaotic, *x* coupled Rössler oscillators. What we see is that the highest spatial frequency mode (*k*=10) goes unstable *before* the lowest mode (*k*=1) becomes stable. This is a result of the scaling relation compressing the highest mode's stability diagram. This will happen eventually in any chaotic system that experiences a SWB if we couple in enough oscillators.

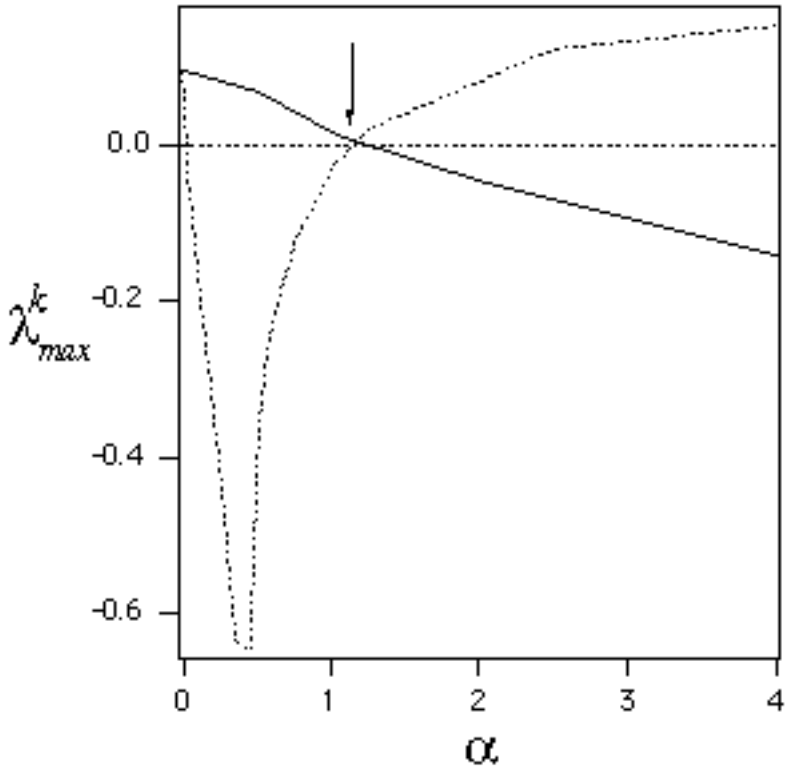

Fig. 8 Stability diagram for modes 1 and 10 of a 20 chaotic Rössler array with *x*-coupling showing the origin of the size limit on synchronizable chaotic oscillators which have short-wavelength bifurcations.

We immediately deduce from this that any chaotic system with a SWB has a limit on the number of oscillators that can be DC and retain a stable, synchronous chaotic state [36]. Above a certain number the highest frequency mode will become unstable before the lowest frequency mode becomes stable as the coupling increases. In fact, we showed that given the zero crossings

of λ^{1}_{max} for mode 1 (say, α_1 and α_2) an expression exists for the largest number of oscillators that can be coupled in stable synchronous behavior [36]. The highest frequency mode is associated with the wave number $k=n/2$. From the scaling relation we have $\lambda^{n/2}_{max}(\alpha_2) = \lambda^{1}_{max}((\gamma_{n/2}/\gamma_1)\alpha_2) = \lambda^{1}_{max}(\alpha_1)$. Solving for n we get the maximum number of oscillators we can couple and still retain synchronization (although the synchronous state may be neutral, depending on the values of α_1 and α_2)

$$n_{\max} = \left[\left[\frac{\pi}{\mathrm{Arcsin}(\sqrt{\alpha_1/\alpha_2})}\right]\right], \tag{13}$$

where by [[.]] we mean integer part of. For example, for the Rössler x-coupling case we have $\alpha_1=0.1232$ and $\alpha_2=4.663$ so that $n_{\max}=19$ in agreement with Fig. 8.

For the limit-cycle situation there is no size limit since λ^{k}_{max} starts at 0 and not some positive number. However, if we go to the continuum limit then there are some consequences. In the continuum limit the coupling constant, as it is used here, must be rescaled by the distance between oscillator sites (nodes) to convert the differences of dynamical variables to second derivatives. We call this distance Δr . It takes the place of the index in Eqs. (3) and scales as $1/n$. The new, continuum coupling becomes $Q=\Delta r^2\alpha$ for x coupling. This rescaling of the coupling causes the higher mode stability diagrams to compress in toward zero coupling. To see this, note that the mode 1 scaling factor Eq. (10) decreases with increasing n, but the Δr^2 factor cancels this decrease exactly in the limit $n \to \infty$. However, the scaling now causes the higher modes to have their stability diagrams compressed toward zero coupling. This means that if we have desynchronizing stability diagrams, the coupling must also go to zero to keep the higher modes stable. Obviously, in the continuum limit we are left with a neutrally stable synchronized state. Thus, even for limit cycle behavior we would not expect to see uniform, stable, synchronized behavior in the presence of a SWB.

Despite what we have just said, there is an intriguing possibility as shown in Fig. 9. In this case we posit that we could have a continuum system in a stable, synchronized limit cycle state

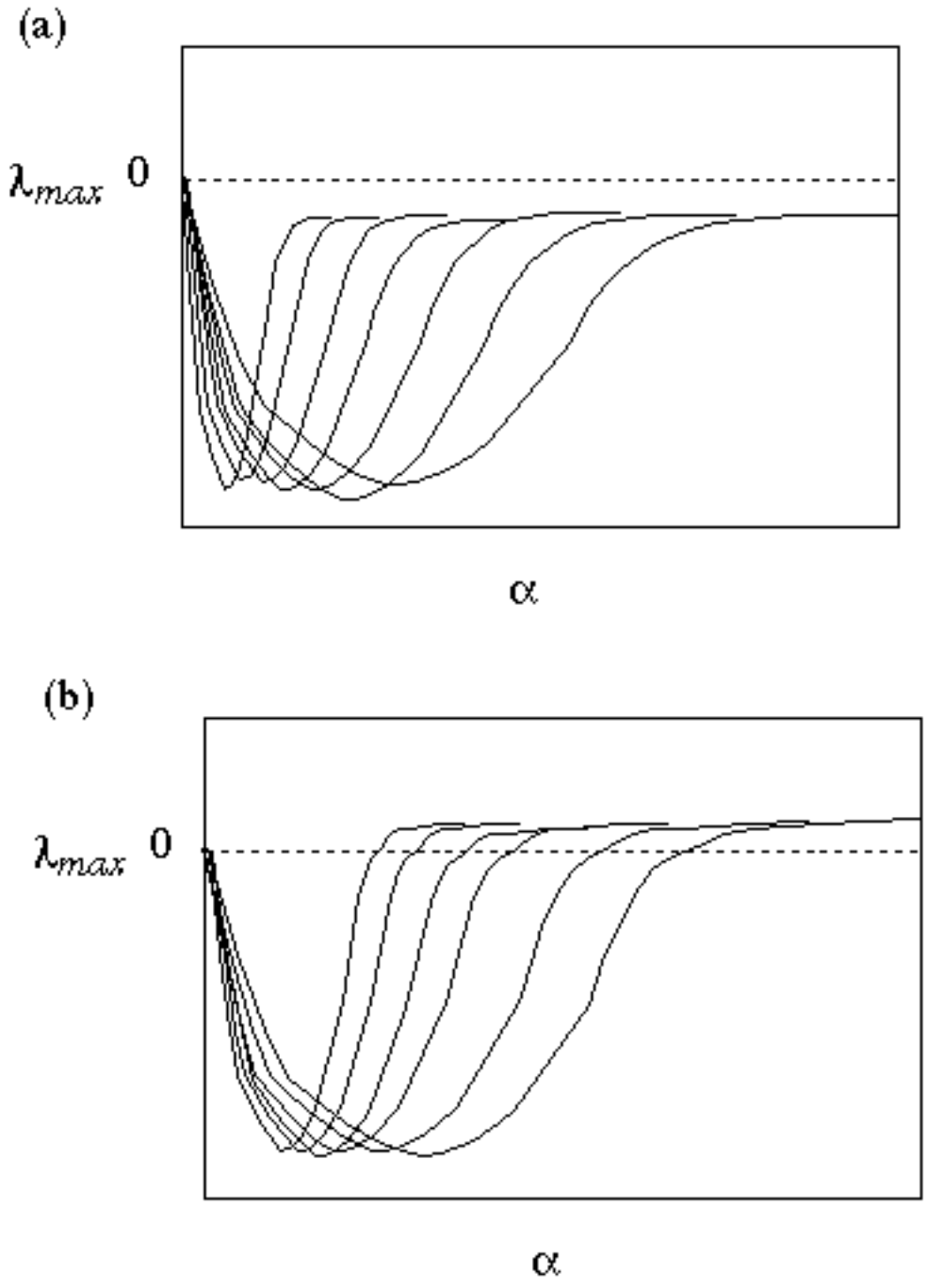

Fig. 9 A possible bifurcation scenario in a continuum system from (a) a stable limit-cycle case to (b) a desynchronizing limit-cycle case.

(Fig. 9 (a)). Then by varying another parameter in the system we cause the stability diagrams to become desynchronizing (Fig. 9 (b)). At any coupling value the first mode to go unstable during

this crossover is the highest spatial frequency. In a continuum system this is theoretically a mode with infinitesimal wavelength, but in practice that wavelength must be finite. The type of bifurcation we are now describing could be a way to probe continuum systems to determine the actual lower limit on wavelengths — that is, what really is the smallest spatial scale of the system? At this point we know of no system that would undergo this bifurcation. We simply put this forth as an interesting possible probe of spatial scales in continuum systems.

III. General Theory of Synchronization Stability in Linearly-Coupled Systems

In this section we want to abstract the essential features from our previous example and see what we can say in general about other systems of linearly coupled oscillators, limit cycles or chaotic systems.

Note that in the motivating example we were able to treat the Jacobian as though the blocks with **J** and **E** were just numbers. This was because we were only operating on each oscillator as a whole when we diagonalized the Jacobian. The Fourier transformation (Eq. (8)) told us to multiply each oscillator component at a site by the *same* number and add this to the same components of other products from other sites. Because we are keeping this separation between the node indices (*i)* and the component indices of each node we can use the mathematical device of direct matrix (tensor) products to express our equations of motion. This allows us to write the equations compactly and keep track of what indices we are operating on.

A. General variational equations for linearly-coupled systems

Let $\mathbf{x}=(\mathbf{x}^{(1)}, \mathbf{x}^{(2)}, ...,\mathbf{x}^{(n)})^T$ be the collection of dynamical variables, where each $\mathbf{x}^{(i)}$ is the dynamical variable vector of *m* dimensions for site *i* (e.g. Eq. (3)). Let $\mathbf{F}=(\mathbf{F}^{(1)}, \mathbf{F}^{(2)}, ...,\mathbf{F}^{(n)})^T$ be the collection of vector fields of the same functional form.. Then, if we assume no coupling, the equations of motion are $\dot{\mathbf{x}}=\mathbf{F}(\mathbf{x})$ with all nodes acting independently. We write the coupling terms using the direct product (our notation is fairly standard here and similar to Wu and Chua [40]):

$$\dot{\mathbf{x}} = \mathbf{F}(\mathbf{x}) + \alpha(\mathbf{G} \otimes \mathbf{E})\mathbf{x}, \tag{14}$$

where **G** is an n×n matrix which determines node-to-node coupling, **E** is an m×m matrix which operates on each node's dynamical vectors to determine which of the oscillator components are coupled, and α determines the relative size of the coupling. We will call the n-dimensional space that **G** operates on the *node space* and the m-dimensional space of each oscillator the *oscillator space*. Without loss of generality we will assume that the rows of **G** all sum to zero:

$$\sum_{j=1}^{n} G_{ij} = 0 \tag{15}$$

for all i. We also take **G** to be symmetric here for simplicity, although generalizations are mentioned in the conclusions.

In our DC x-coupling example we would have

$$\mathbf{G} = \begin{pmatrix} -2 & 1 & 0 & \cdots & 1 \\ 1 & -2 & 1 & \cdots & 0 \\ \vdots & \vdots & \vdots & \vdots & \vdots \\ 1 & \cdots & 0 & 1 & -2 \end{pmatrix} \quad \text{and} \quad \mathbf{E} = \begin{pmatrix} 1 & 0 & 0 \\ 0 & 0 & 0 \\ 0 & 0 & 0 \end{pmatrix}, \tag{16}$$

The Fourier transform would then act on only **G** and on each $\mathbf{x}^{(i)}$ and $\mathbf{F}^{(i)}$ as a whole. In fact, to be consistent, we really should write each "unit vector" in Eq. (8) not as $\mathbf{e}_j$, but as $\mathbf{e}_j \otimes \mathbf{1}_m$, where $\mathbf{e}_j$ is an n-dimensional vector of all zeroes except for a 1 in the ith position and $\mathbf{1}_m$ is the m×m unit matrix. Then the $\{\mathbf{e}_j\}$ are a basis only for the node space that supports **G**. However, because of the separation of the node and oscillator spaces we need not be so formal so long as we are careful to distinguish which space we are operating on.

To study the stability of the synchronized state we need the variational equation derived from Eq. (14):

$$\dot{\xi} = [D\mathbf{F}(\mathbf{x}) + \alpha(\mathbf{G} \otimes \mathbf{E})]\xi = [\mathbf{1}_n \otimes \mathbf{J} + \alpha(\mathbf{G} \otimes \mathbf{E})]\xi, \tag{17}$$

where $\mathbf{1}_n$ is an n×n identity matrix and $\mathbf{J}$=$D\mathbf{F}^{(i)}$ is the Jacobian in the oscillator space evaluated on the synchronization manifold. Because of synchronization **J** is the same for all i.

B. Diagonalization of the array Jacobian: Getting exact expressions

If we examine the problem of diagonalizing the **G** matrix, we can often accomplish that using purely numerical methods. This can be done and the results of the scaling relations developed later will carry through for those cases, too. However, in this section we would like to examine diagonalization methods that lead to explicit expressions for the eigenvalues of **G** so we can comment on their dependence on system size, n.

One approach to diagonalizing the right-hand-side of Eq. (17) is to look for symmetries. In our DC example it was a shift symmetry in the node space that led us to the use of the Fourier transformation to get a block diagonalization. That block diagonalization essentially came from a diagonalization of **G** which along with the already diagonal $\mathbf{1}_n$ gave the equations (11) with γ_k as an eigenvalue of **G.**

We use the same approach here and it will lead us to an application of group representation theory. Our intention here is to motivate this approach. The use of group theory in such contexts is not well known in the nonlinear dynamics community and here we want to call attention to its usefulness. We then show the results for several different coupling schemes. We will not go into the details of all the group theoretic issues, although we do show one simple example in Appendix A. More detailed issues involving groups and dynamics can be found in [46, 64-68], although we do not know of any publication which shows the interplay between the coupling scalings (the **G** eigenvalues) and the stability diagram as we show here.

In the uncoupled array if we permute the nodes in any fashion (interchange various (i) indices), then we will not affect the dynamics. Such a permutation will lead to a similarity transformation on the node components of the first term in Eq. (17). Since the unit matrix $\mathbf{1}_n$ commutes with all nxn matrices any permutation operation has no effect on this first term. In group theoretic terms the first term is invariant under actions of the symmetric group (S_n) acting on the node space. When we include the coupling (the second terms in Eq. (17)) we may not have a variational equation that is invariant under S_n. A good question is, what, if any, invariance does the second term have? Is there a subset of permutations (a subgroup of S_n) under which the term is invariant. In our DC example the subgroup was the set of shift permutations.

The reason why the search for a group of invariant operations is so useful in diagonalizing Eq. (17) comes from Schur's lemma [46, 64-68]. A finite group has a finite number of irreducible representations (matrix sets with the same rules as the group). Irreducible representation (IR) means there is no linear transformation that will break the representation into two or more lower-dimensional representations. If we can find what IR's are present in our system and transform to their coordinate systems then we can use the lemma:

> Schur's Lemma: Any matrix which commutes with all matrices of an irreducible representaion must be a constant matrix (i.e. a multiple of $\mathbf{1}_d$, where d is the dimension of the irreducible representation matrices).

If our matrix **G** is invariant under the group, then **G** qualifies as the commuting matrix of the lemma. This means that, in the coordinate systems of the IR's, **G** will be block diagonalized into blocks each the size of one of the IR's. This process can be viewed as a generalized kind of diagonalization imposed by symmetry. If the IR appears more than once say, l times, then the block in **G** associated with that IR has dimension ld, where d is the IR dimension. If the IR appears only once then the block is just a multiple of $\mathbf{1}_d$ and the multiple (which we call γ_k) is the eigenvalue of that block. If the IR appears more than once, we can still diagonalize that particular block by other means. The important point is that we have reduced the dimension of the diagonalization problem to smaller blocks.

The facts of the previous paragraphs can be found in any good book on applications of group theory and representations [46, 64-68]. The only step often left out is actually finding the basis of the IR in the node space. This is important to achieve actual diagonalization and find the γ_k,. We show one approach to this step in Appendix A using projection operators.

We bring the synchronization manifold into this discussion by noting that because of Eq. (15) 0 is an eigenvalue of **G** and the synchronization manifold as given by the first equation in Eq. (8) is the subspace associated with that eigenvalue. Hence, we choose $\gamma_0=0$ which causes Eq. (11) to revert to the variational equation for the isolated system as in our example. In group theory

terms this manifold is always associated with the trivial IR (1-dimensional matrices equal to the number 1). Other IR's and eigenvalues will be associated with motions transverse to the synchronization manifold. Thus, as in the DC example we want the variational equations associated with those motions to be damped out (i.e. to have negative Lyapunov or Floquet exponents). We will follow convention and call the transverse motions modes, which can be thought of as a generalization of our Fourier modes from our example. We do note (as shown in Appendix A) that the trivial IR can also appear more than once and in those cases the extra appearances will be associated with other transverse modes, i.e. the trivial IR is not uniquely identified with the synchronization manifold.

C. General scaling relations

Once we have diagonalized **G** we can break Eq. (17) into separate blocks of uncoupled variational equations like Eq. (11). In each equation we will, in general, have a different eigenvalue γ_k of **G**, where k=0,...,K-1 with K being the number of eigenvalues found which will be greater than or equal to the number of different IR's found. Observe that all the equations will have the same form as Eq. (11), independent of what form of **G** we started with. Only the eigenvalues will change. We can now generalize our scaling statements for the DC example to the following:

Linear Coupling Scaling Relation: For a fixed choice of dynamics ($\mathbf{F}^{(i)}(\mathbf{x})$) and oscillator component couplings (**E**), if we can diagonalize the coupling matrices **G** and **G'** in two arrays of identical, synchronized nodes, each with possibly different number of oscillators, then the stability diagram given by the Lyapunov (or Floquet) exponent $\lambda^{k}_{max}(\alpha)$ for the kth mode of a coupling **G** is related to that given by the qth mode for any other coupling **G'** by the scaling relation $\lambda^{k}_{max}(\alpha)=\lambda^{q}_{max}((\gamma_k/\gamma'_q)\alpha)$, where γ_k is the eigenvalue of **G** associated with the kth mode and γ'_q is an eigenvalue of **G'** associated with the qth mode**.**

Given our experiences with various desynchronizing bifurcations and other array size limits in DC systems, we might conjecture that similar behavior could result in other types of coupled systems. This turns out to be true. In the next section we will investigate the stability of

synchronized behavior in arrays of limit cycle and chaotic nodes using several other coupling schemes.

Fig. 10 The coupling scheme for open-ended diffusively-coupled nodes.

IV. Results for Other Couplings

A. Open-ended diffusively coupled nodes

Fig. 10 shows this coupling scheme which gives the **G** matrix

$$\mathbf{G} = \begin{pmatrix} -1 & 1 & 0 & \dots & 0 \\ 1 & -2 & 1 & \dots & 0 \\ \vdots & \vdots & \vdots & \vdots & \vdots \\ 0 & \dots & 0 & 1 & -1 \end{pmatrix}. \tag{17}$$

We showed in [3] as did Armbruster and Dangelmayr [47] that this matrix can be diagonalized in a manner similar to the shift-invariant, DC case using a discrete Fourier transform with n replaced by $2n$. The results give the eigenvalues

$$\gamma_k = -4\sin^2\left(\frac{\pi k}{2n}\right), \text{ for } k = 0,1,\dots,n-1. \tag{18}$$

This is just like the original DC example, except that there are no degenerate modes and the highest wavelength is for k=n-1. Nonetheless, because of the dependence of the eigenvalues on n and the scaling law we will see the same phenomena as before. If mode 1 has a desynchronizing bifurcation, Limit cycle arrays will have their region of stable coupling compressed toward zero — leaving a neutrally-stable continuum case. Chaotic arrays will have a limit on the number of nodes that can be coupled in stable synchronous behavior:

$$n_{\max} = \left\lfloor \frac{\pi}{2\,\mathrm{Arctan}(\sqrt{\alpha_1/\alpha_2})} \right\rfloor \tag{19}$$

For example, for the Rössler *x*-coupling case we already know α_1 and α_2, so using Eq. 16 have N_{max}=9. Thus for the same coupling components (*x*) the open-ended DC can support fewer chaotic oscillators in the synchronized state than the ring-coupled DC.

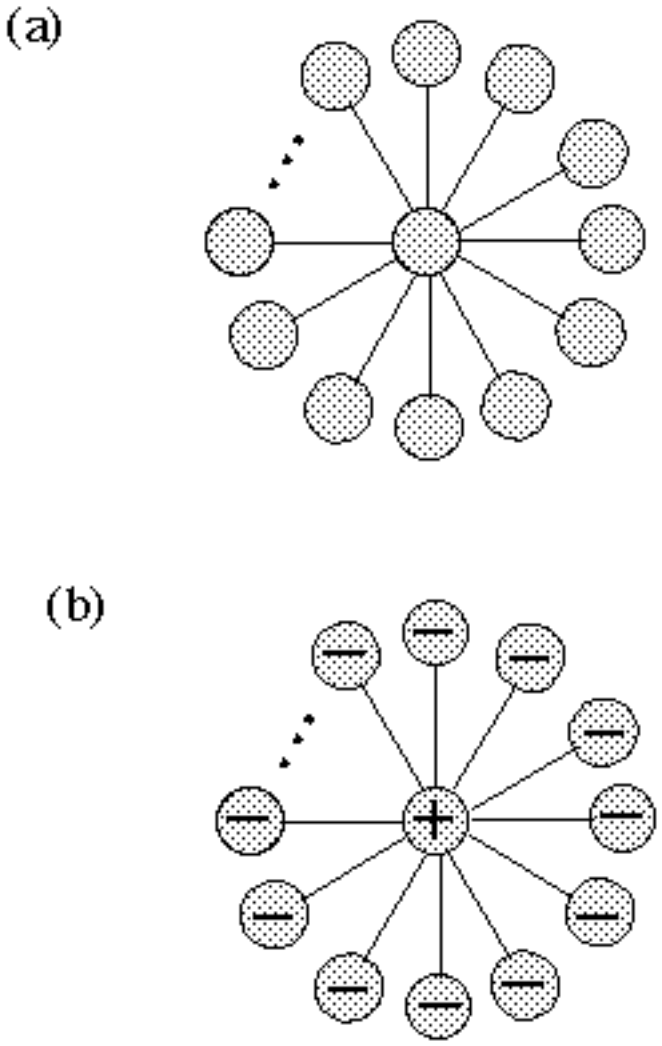

Fig. 11 (a) The coupling scheme for star-coupled nodes. (b) The highest "frequency" mode for the star-coupled array.

B. Star configuration of coupled nodes

Here, as shown in Fig. 11 (a) we have a node at a central hub position and all other nodes come off from that one. The coupling matrix is

$$\mathbf{G} = \begin{pmatrix} n-1 & 1 & 1 & \cdots & 1 \\ 1 & -1 & 0 & \cdots & 0 \\ 1 & 0 & -1 & \cdots & 0 \\ \vdots & \vdots & \vdots & \vdots & \vdots \\ 1 & 0 & 0 & \cdots & -1 \end{pmatrix}. \qquad (20)$$

Using the group theory methods of Appendix A it is straightforward to show that the mode eigenvalues for n oscillators are

$$\gamma_k = -1, \text{ for } k = 1,\ldots,n-2 \quad \text{and} \quad \gamma_{n-1} = -n. \qquad (21)$$

The modes k=1,...,n–2 represent directions transverse to the synchronization manifold in which the oscillators of the star go out of sync with the hub in waves wrapping commensurately around the star. The highest mode (k=n–1) represents a mode in which all outer nodes are in sync with each other, but out of sync with the hub (see Fig. 11 (b)).

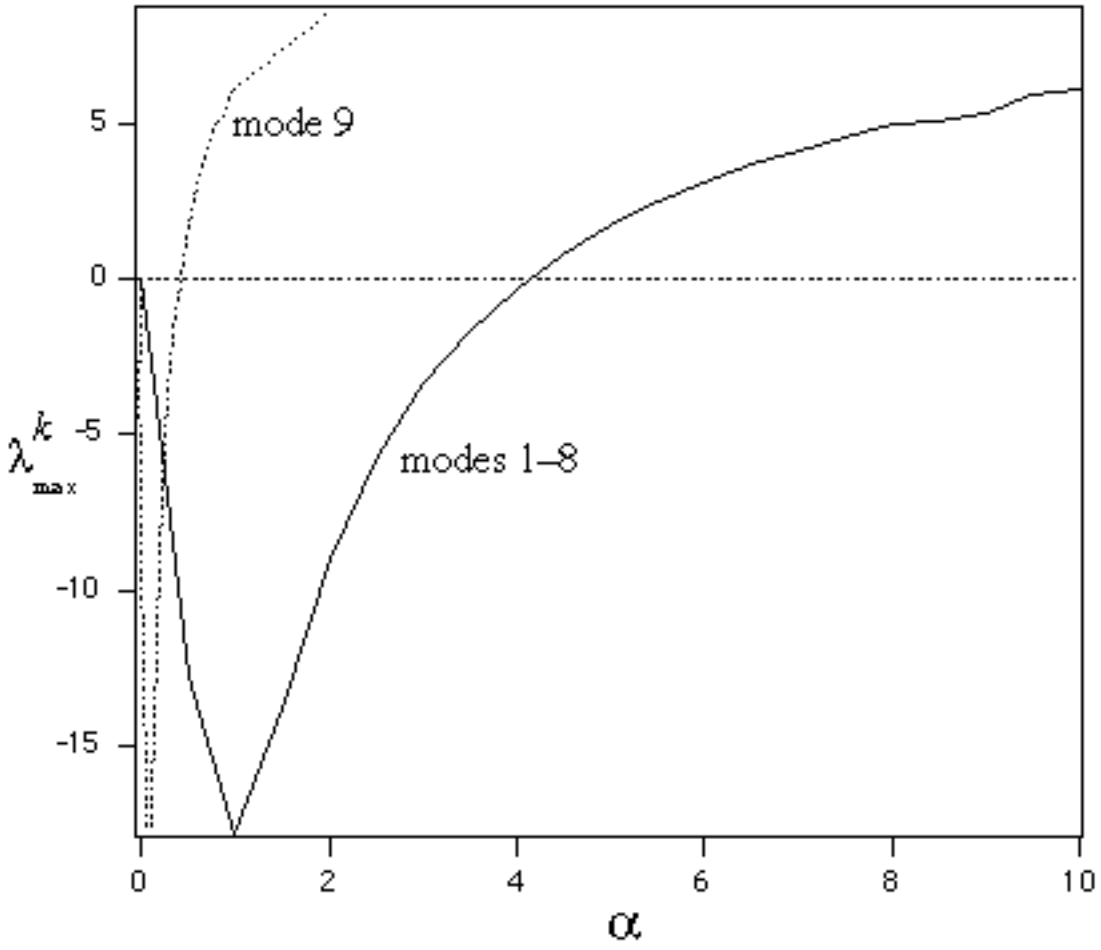

Fig. 12 Stability diagram for modes 1 through 9 of a 10 limit cycle star-Rössler array with *x*-coupling. Modes 1-8 are solid line and have the same stability. The desynchronizing bifurcation arises from the *k*=9 mode (the dotted line), the "drum-head vibration."

In Fig. 12 we see the stability diagram for 10 star-*x*-coupled limit cycle Rössler oscillators. We have the desynchronization bifurcation as coupling increase, although in this case the first mode to go unstable is more like a vibrating *drum-head mode*, rather than a SWB. In Fig. 13 the same diagram for 35 star-*x*-coupled chaotic Rössler oscillators shows that this coupling scheme also has a size limit on stable, synchronized chaotic behavior. Similar to the DC array case it is the monotonic decrease of the eigenvalue ratio $\gamma 1 / \gamma n\text{-}1$ with *n* that causes the stability diagrams for different modes to cross and prevent stable, synchronized chaos. In this case,

$$n_{\max} = \left[\left[\alpha_2 / \alpha_1\right]\right] \qquad (22)$$

For the Rössler *x*-coupling case we have $n_{\max}$=35 which is far larger than either open-ended DC or ring-DC schemes.

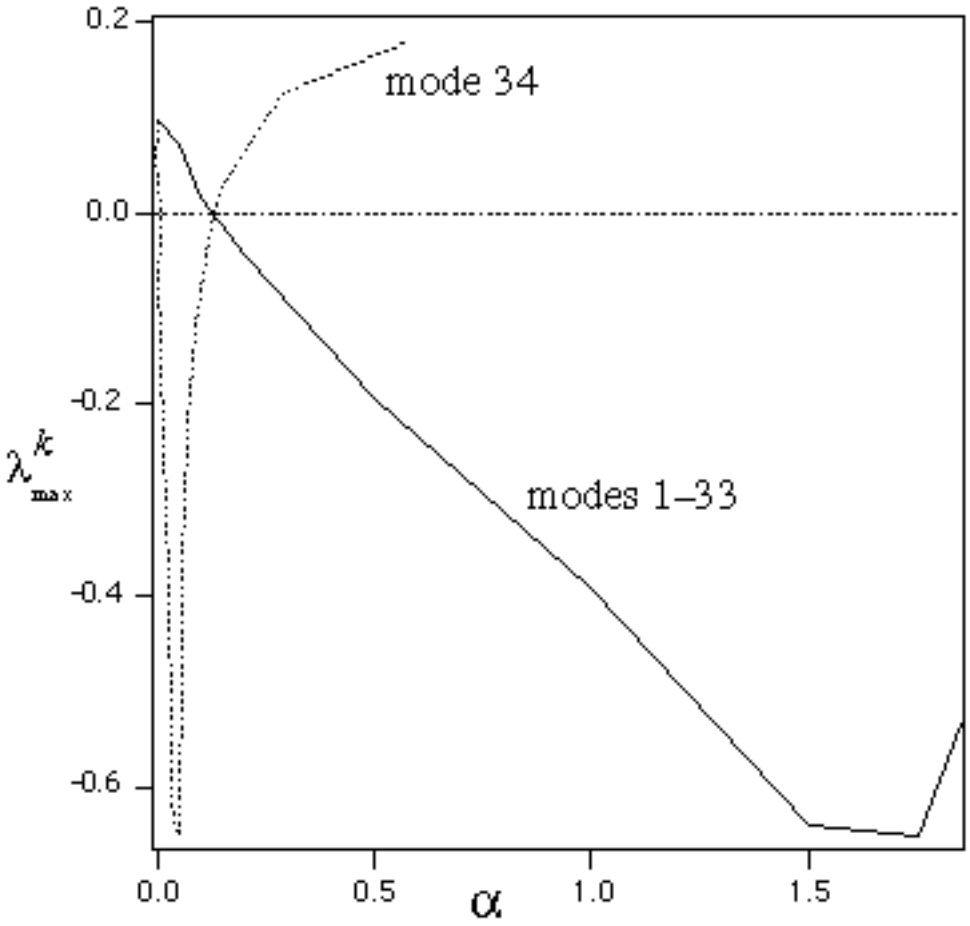

Fig. 13 Stability diagram for modes 1 through 34 of a 35 chaotic star-Rössler array with *x*-coupling showing the size limit coming as the *k*=34 mode goes unstable just as the 1-33 modes go stable.

C. All-to-all coupled nodes

This is a coupling type in which all nodes are coupled to each other through an average over the particular coupling component. It is a coupling assumed in many biological systems [23, 24, 28, 29] and in the study of Josephson-junction arrays [7, 25, 29, 69-72]. The coupling matrix is

$$\mathbf{G} = \begin{pmatrix} -n+1 & 1 & 1 & \cdots & 1 \\ 1 & -n+1 & 1 & \cdots & 1 \\ 1 & 1 & -n+1 & \cdots & 1 \\ \vdots & \vdots & \vdots & \vdots & \vdots \\ 1 & 1 & 1 & \cdots & -n+1 \end{pmatrix}. \qquad (23)$$

This matrix has the complete symmetry of the symmetric group S_n and can be diagonalized easily. A discrete Fourier transform will do. We get for the eigenvalues $\gamma_1 = -n$ for all $k > 0$. In this case the stability diagrams for all transverse modes are the same. Even in systems with desynchronizing bifurcations there will be no collapse of the stability region to zero in the limiting case for periodic oscillators, nor will there be a size limit to a synchronizable chaotic array. We can have a synchronized system for any coupling value below the desynchronization threshold, which is the same for all modes. To put it another way, at the desynchronization threshold all modes go unstable simultaneously.

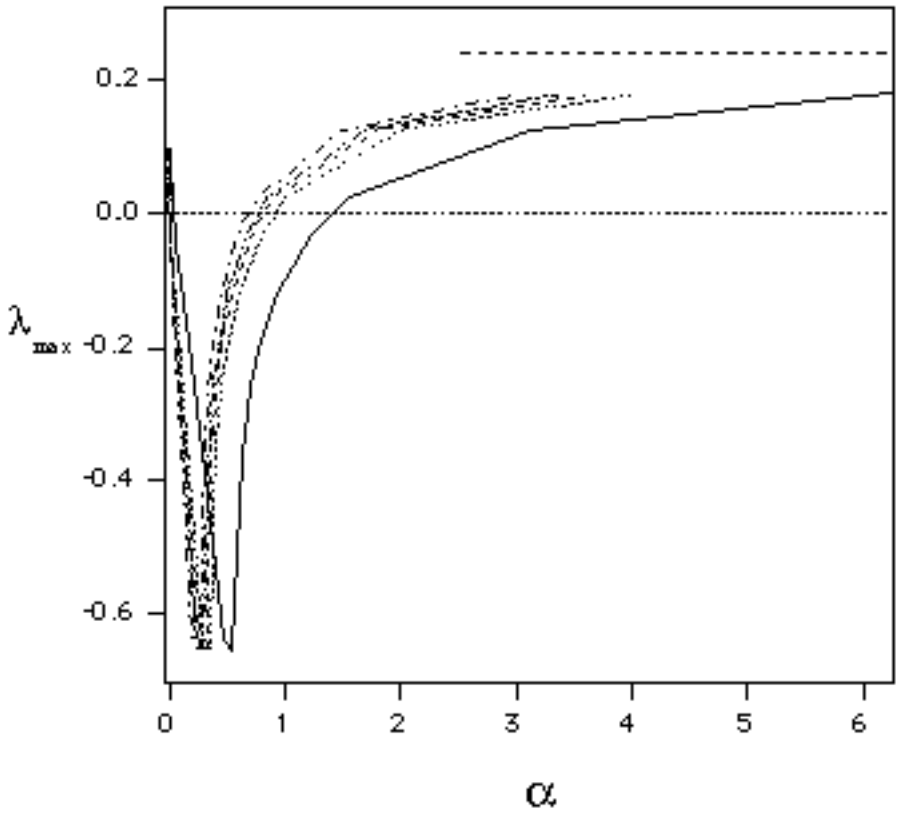

Fig. 14 Stability diagram for modes 1 through 5 of a 6 chaotic randomly-coupled Rössler array with *x*-coupling.

D. Random, Symmetric Coupling

We can also generate random, symmetric couplings using the following formulas for components of **G**: $G_{ij}= \omega$ for $i > j$, $G_{ij}=G_{ji}$ for $i < j$, and $G_{ii} = -\sum_{j\neq i} G_{ij}$, where ω is a uniformly distributed random number from 0 to 1. This formulation guarantees a zero eigenvalue (for the synchronization manifold) and other eigenvalues all negative. There are no symmetries so we solve for the eigenvalues numerically. In Fig. 14 we see the stability diagram for 6 *x*-coupled Rössler oscillators. In this case we have coupling regimes in which global synchronization is possible. However, unlike the other cases we have studied so far, the random coupling could yield a non-synchronizable situation at potentially any number of oscillators — we have no symmetry to aid us in finding a formula for the eigenvalues γ_k.

Fig. 15 shows the modes corresponding to the stability funcitons in Fig. 14. We see that they do not resemble the sine and cosine modes we've studied, except for the synchronized mode, k=0.

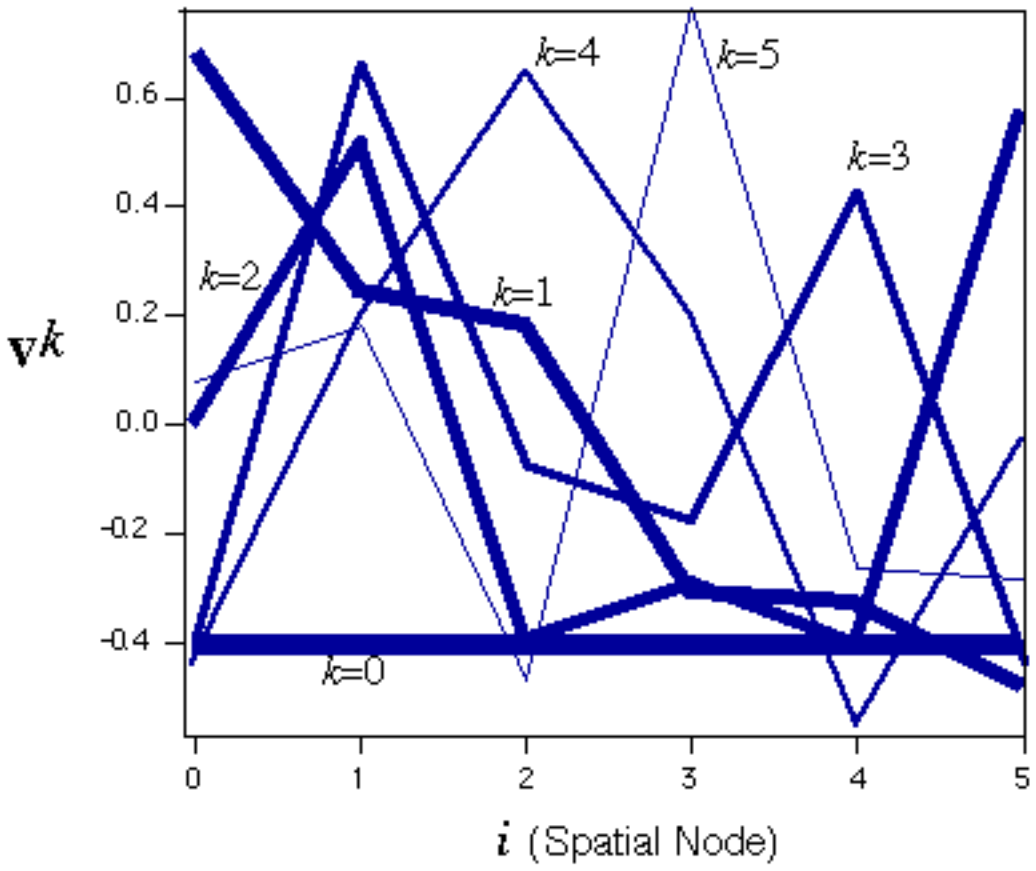

Fig. 15 Spatial dependencies of modes for the 6 chaotic randomly-coupled Rössler array with *x*-coupling.

V. On a Conjecture on Synchronization Criteria

Recently, Wu and Chua [40] put forth a conjecture on a criterion for synchronization in an array of linearly coupled oscillators. This conjecture involves a relation between the coupling eigenvalues and the coupling constant in arrays of various sizes. With our developments in this paper we are able to comment conclusively on the conjecture. The conjecture is as follows:

If we have two arrays of linearly coupled oscillators with n_1 and n_2 oscillators in each array, with coupling matrices $\mathbf{G}_1$ and $\mathbf{G}_2$ and coupling strengths α_1 and α_2, then if $\gamma(1)$ and $\gamma(2)$ are the least negative nonzero eigenvalues of $\mathbf{G}_1$ and $\mathbf{G}_2$ respectively and the coupling strengths are such that

$$\alpha_1 \gamma(1) = \alpha_2 \gamma(2) \qquad (24)$$

then array 1 globally synchronizes if and only if array 2 globally synchronizes.

Wu and Chua go on to show supporting numerical evidence for this relation using several systems like those in section IV above for many different array sizes, *n*. The numerical experiments are conducted on the double-scroll oscillator [73, 74] and show that for a large range of *n* values the products $\alpha\ \gamma$ (as in Eq. (24)) taken at the threshold for synchronization are roughly constant. As Wu and Chua point out this could mean we can predict the synchronization of an array of any size for a chosen **G** just by knowing whether one such array synchronize (e.g. test for synchronization when *n*=2).

Given our findings above on size limits in chaotic arrays which have desynchronization bifurcations we can immediately state that the above conjecture must be false, in general. But we can still ask why Wu and Chua saw the numerical relations they did. The answer is that Eq. (24) holds for the stability of the least stable mode. That is, if we increase the coupling from zero our scaling relation shows that the last mode to go stable is the mode associated with the smallest, nonzero eigenvalue of **G**. Call this mode 1 (as we did for our DC examples). Then we have $\lambda^{k}_{max}(\alpha_1)=0$ at the synchronization threshold for a mode *k* in array 1 and $\lambda^{q}_{max}(\alpha_2)=0$ at the synchronization threshold for a mode *q* in array 2. By the scaling relation we have

$$\alpha_2 = \frac{\gamma_k(1)}{\gamma_q(2)}\alpha_1 \qquad \alpha_2\gamma_q(2) = \alpha_1\gamma_k(1), \qquad (25)$$

which is precisely the Wu and Chua relation, except that it pertains to the stability of individual modes. In using the smallest, nonzero eigenvalues Wu and Chua were choosing the least stable modes to test, assuming that when it was stable all other modes would remain stable, too. In cases of desynchronization, the latter assumption can fail. In many coupling schemes (like DC) this is the last mode to become stable as the coupling increase from zero and in those cases where there is no desynchronization it can serve as a guide to global synchronization. Of course, given the scaling relation we have presented, any mode can serve as the guide.

VI. Conclusions and Remarks

We have shown that given a fixed, chosen component coupling **E**, the stability diagram for many coupling schemes as represented by the matrix **G** in the node space can be calculated by knowing only one diagram for a particular coupling scheme. For example, it suffices to know the stability diagram for two DC oscillators. All other stabilty diagrams for any symmetric coupling of any number of those oscillators can be calculated from that one.

When considering the stabilty of the synchronous state for the whole array one must be careful to examine the stability diagrams to make sure that *all* modes are stable at the chosen coupling. This is the downfall of the Wu and Chua conjecture, although the conjecture is true if applied to individual modes.

An area we have only touched upon is that of dynamical systems with random, linear coupling. Such systems are often used in neural networks [75], map lattices [76, 77], and spin-glass systems [78]. When the individual units are nonlinear desynchronization behavior can occur and we must examine the mode stability diagrams as in this paper. Questions regarding percoltion thresholds and probability of desynchronization, among others, can be treated with the present approach. A distribution of couplings will lead to a distribution of scalings of the mode stability curves. The consequences of this are still not clear.

We can also work with coupling matrices **G** which are not symmetric and even those which are calculated numerically (e.g. from random, linear coupling schemes). These will, in general, have complex eigenvalues. In this case we must calculate the surface over the complex plane $\mathbb{C}$ defined by a the exponents $\lambda_{max}(\alpha)$, where now α is complex. Now when we rescale the coupling by γ_k/γ'_q we will, in general, have a complex number which will give, in general, a complex coupling whose value of λ_{max} we get from our surface. Once again, we have reduced the problem to one of calculating $\lambda_{max}(\alpha)$ for one scheme (e.g. two oscillators) once and for all. We are left with the question, is there any physical meaning to the complex coupling values? At this point we have no general answer to this question, although we are continuing to work on this general case [79].

Acknowledgments

I would like to acknowledge many conversations about the synchronization problem in coupled systems with James F. Heagy and Thomas L. Carroll. I would also like to acknowledge several helpful suggestions by one of the referees, especially in pointing out other possible links to randomly coupled systems.

Appendix A. Diagonalization of a Star-Coupling Matrix

What we want to do here is show how one goes about block-diagonalizing a matrix that is invariant under a group of transformations. Other methods may also work, but the use of symmetry is algorithmic and guaranteed to accomplish some level of block diagonalization. It also can often lead to explicit formulas for the eigenvalues which are useful, for example in calculating $n_{\max}$.

To use the group methods we must (1) find the symmetry group associated with the star-coupling configuration, (2) write down the matrices that represent the operations of that group in the node space, (3) find out which irreducible representations (IR) are present in those matrices, and (4) transform to the coordinate systems of those IR's. The last step will block-diagonalize the node coupling matrix **G**. We show an example of this for n=5. In Fig. 11 (a) we see that a star configuration will have a rotational symmetry: We can rotate by $2\pi/(n-1)$ or equivalently shift the outer ring by one and the configuration doesn't change. The symmetry group generated by these operations is the C_4 point group. This group has 4 IR's (A, B, E_1, E_2). The character table is shown in Table I.

Table I here.

In Table I we have used the sine and cosine version of the E representations and C_4 is a shift by one, C_2 a shift by 2, and C_4^3 a shift by three oscillators. This is step (1).

The transformation matrices (step (2)) that represent the group shift operations in the node space are

$$E = \begin{pmatrix} 1 & 0 & 0 & 0 & 0 \\ 0 & 1 & 0 & 0 & 0 \\ 0 & 0 & 1 & 0 & 0 \\ 0 & 0 & 0 & 1 & 0 \\ 0 & 0 & 0 & 0 & 1 \end{pmatrix}, \quad C_4 = \begin{pmatrix} 1 & 0 & 0 & 0 & 0 \\ 0 & 0 & 1 & 0 & 0 \\ 0 & 0 & 0 & 1 & 0 \\ 0 & 0 & 0 & 0 & 1 \\ 0 & 1 & 0 & 0 & 0 \end{pmatrix},$$

$$C_2 = \begin{pmatrix} 1 & 0 & 0 & 0 & 0 \\ 0 & 0 & 0 & 1 & 0 \\ 0 & 0 & 0 & 0 & 1 \\ 0 & 1 & 0 & 0 & 0 \\ 0 & 0 & 1 & 0 & 0 \end{pmatrix}, \quad C_4^3 = \begin{pmatrix} 1 & 0 & 0 & 0 & 0 \\ 0 & 0 & 0 & 0 & 1 \\ 0 & 1 & 0 & 0 & 0 \\ 0 & 0 & 1 & 0 & 0 \\ 0 & 0 & 0 & 1 & 0 \end{pmatrix}. \qquad (26)$$

The vector of characters (matrix traces) for these transformations is **u**=(5,1,1,1). We now use the standard orthogonality relations for IR's [65-68] to find out which IR's are present: if **v** is the vector of characters for the *k*th IR, then the number of times this IR appears in the transformation matrices is given by (**u**•**v**)/*N*, where *N* is the order of the group (4 here). Using this formula we see that the *A* (trivial) representation is present twice, and all other IR's are present once. The degeneracy in *A* will show up as an undiagonalized 2×2 block, which we will diagonalize by other means. We have completed step (3).

We are ready for step (4): diagonalize **G**, Eq. (20). To do this we need to know the basis vectors in our node space of the various IR's (*A*, *B*, E_1, E_2). This construction is not usually covered well in standard group theory representation books. We show here one simple way to go about it.

We can use the transformations (Eq. (26)) along with the IR characters to form projection operators onto the subspaces associated with each IR [65-68]. The projection operator for the *k*th IR is

$$P_k = \frac{l_k}{N} \sum_{i=1}^{N} v_i T_i , \qquad (27)$$

where v_i is the *i*th component of the trace vector **v** associated with the *k*th IR, T_i is the node-space transformation associated with the *i*th group operation (e.g. Eq. (26)), and l_k is the dimension of the *k*th IR. The application of the projection operator will project out of any vector that part

which is contained in the subspace spanned by the basis of that particular IR. For example applying the *B* IR projection to (0,1,0,0,0) we get (0,1,–1,1,–1). Since this IR is one-dimensional we can normalize this vector and it is the basis for the *B* IR. For higher-dimensional IR's we can orthonormalize the set of vectors projected into the subspace. We do similar operations on other 5-dimensional vectors and we obtain the basis for all the IR subspaces. Note that the subspace for the *A* IR is 2-dimensional. Hence, we have some flexibility to choose any two basis vectors in that subspace.

Table I

IR	E	C_4	C_2	C_4^3
A	1	1	1	1
B	1	–1	1	–1
E_1	1	–1	–1	1
E_2	1	1	–1	–1

Table I. Characters for the irreducible representations of the C_4 point group.

We put all the basis vectors together to form a transformation matrix that will take us from the standard node-space basis ($\mathbf{e}_i$) to the IR basis:

$$S = \frac{1}{2}\begin{pmatrix} \sqrt{2} & 0 & 0 & 0 & 0 \\ 0 & 1 & 1 & 1 & 1 \\ 0 & 1 & -1 & 1 & -1 \\ 0 & 1 & -1 & -1 & 1 \\ 0 & 1 & 1 & -1 & -1 \end{pmatrix}. \qquad (28)$$

Then calculating the induced similarity transformation $S\mathbf{G}S^{-1}$ we have a block-diagonalized coupling matrix:

$$\mathbf{D}' = \begin{pmatrix} -4 & 2 & 0 & 0 & 0 \\ 2 & -1 & 0 & 0 & 0 \\ 0 & 0 & -1 & 0 & 0 \\ 0 & 0 & 0 & -1 & 0 \\ 0 & 0 & 0 & 0 & -1 \end{pmatrix}. \tag{29}$$

The block in the upper-left-hand corner is associated with the trivial *A* IR. One eigenvector of this block will be associated with the synchronization manifold (with zero eigenvalue), the other will be associated with the highest frequency mode of Fig. 11 (b). This confirms our statement in the text that the association of the trivial IR with the synchronized state is not unique.

We can easily complete the diagonalization of (29) in the remaining block and get

$$\mathbf{D} = \begin{pmatrix} 0 & 0 & 0 & 0 & 0 \\ 0 & -5 & 0 & 0 & 0 \\ 0 & 0 & -1 & 0 & 0 \\ 0 & 0 & 0 & -1 & 0 \\ 0 & 0 & 0 & 0 & -1 \end{pmatrix}. \tag{30}$$

Using the same approach we can easily show that for *n* nodes in the star configuration we will get

$$\mathbf{D} = \begin{pmatrix} 0 & 0 & 0 & \cdots & 0 \\ 0 & -n & 0 & \cdots & 0 \\ 0 & 0 & -1 & \cdots & 0 \\ \vdots & \vdots & \vdots & \vdots & \vdots \\ 0 & 0 & 0 & \cdots & -1 \end{pmatrix} \tag{31}$$

which confirms the eigenvalues we used in the star-coupled example.

References

[1] J. M. Kowalski, G.L. Albert, and G. W. Gross, Physical Review **A 42**, 6260 (1990).

[2] T. Kapitaniak, Physical Review **E 47**, R2975 (1993).

[3] J.F. Heagy, T.L. Carroll, and L.M. Pecora, Physical Review **E 50** (3), 1874 (1994).

[4] H.G. Winful and L. Rahman, Physical Review Letters **65** (13), 1575 (1990).

[5] V. Pérez-Villar, A.P. Muñuzuri, V. Pérez-Muñuzuri *et al*., International Journal of Bifurcations and Chaos **3** (4), 1067 (1993).

[6] P. Ashwin, J. Buescu, and I. Stewart, Physics Letters **A 193**, 126-139 (1994).

[7] N. Nakagawa and Y. Kuramoto, Progress of Theoretical Physics **89** (2), 313 (1993).

[8] J.F. Heagy, T.L. Carroll, and L.M. Pecora, Physical Review Letters **73**, 3528 (1995).

[9] Chai Wah Wu and Leon O. Chua, International Journal of Bifurcations and Chaos **4** (4), 979 (1994).

[10] J.F. Heagy, T.L. Carroll, and L.M. Pecora, Physical Review **E 52** (2), R1253 (1995).

[11] D.J. Gauthier and J.C. Bienfang, Physical Review Letters **77** (9), 1751 (1996).

[12] L. Pecora, T. Carroll, and J. Heagy, *Chaotic Circuits for Communications, Photonics East, SPIE Proceedings*, Philadelphia, 1995, **2612**,25-36 (SPIE,Bellingham WA USA)

[13] L.S. Tsimring and M.M. Sushchik, Physics Letters **213** (3-4), 155-166 (1996).

[14] V.Pérez-Villar, A.P. Muñuzuri, V.Pérez-Muñuzuri *et al*., International Journal of Bifurcations and Chaos **3** (4), 1067-1074 (1993).

[15] M.N. Lorenzo, I.P. Marino, V. Pérez-Muñuzuri *et al*., Physical Review **54** (4), R3094 (1996).

[16] L. Kocarev and U. Parlitz, Physical Review Letters **77**, 2206- 2209 (1996).

[17] J.H. Xiao, G. Hu, and Z. Qu, Physical Review Letters **77** (20), 4162 (1996).

[18] K. M. Cuomo, International Journal of Bifurcations and Chaos **3** (5), 1327-1337 (1993).

[19] H. Fujisaka and T. Yamada, Progress of Theoretical Physics **69** (1), 32 (1983).

[20] T. Yamada and H. Fujisaka, Progress in Theoretical Physics **70**, 1240 (1983).

[21] V.S. Afraimovich, N.N. Verichev, and M.I. Rabinovich, Inv. VUZ. Rasiofiz. RPQAEC **29**, 795-803 (1986).

[22] A.R. Volkovskii and N.F. Rul'kov, Sov. Tech. Phys. Lett. **15**, 249 (1989).

[23] N. Kopell and G.B. Ermentrout, Math. Biosciences **90**, 87 (1988).

[24] Y. Kuramoto, "Self-entrainment of population of coupled nonlinear oscillators," in *International Symposium on Mathematical Problems in Theoretical Physics, Lecture Notes in Physics*, edited by H. Araki (Springer, Berlin, 1975), Vol. No. 39, pp. 420-422.

[25] S. Watanabe and S.H. Strogatz, Physical Review Letters **70** (16), 2391 (1993).

[26] E.E. Shnol, PMM U.S.S.R. **51** (1), 9 (1987).

[27] P. Baldi, J. Buhmann, and R. Meir, "Computing with Arrays of Coupled Oscillators," in *Proceedings of the International Neural Network Conference (IEEE)* (Klawer, Newell, MA, 1990), pp. 908-911.

[28] S.H. Strogatz, Biomathematics **100** (1993).

[29] Steven Strogatz, *Nonlinear Dynamics and Chaos* (Addison-Wesley Publishing Co., Reading Massachusettes, 1994).

[30] P. Ashwin, J. Buescu, and I. Stewart, Nonlinearity **9**, 703-737 (1994).

[31] S.C. Venkataramani, B. Hunt, and E. Ott, Physical Review E **54**, 1346--1360 (1996).

[32] S.C. Venkataramani, B. Hunt, and E. Ott, Physical Review Letters **77** (27), 5361 (1996).

[33] J.C. Alexander, J.A. Yorke, Z. You *et al.*, International Journal of Bifurcations and Chaos **2**, 795 (1992).

[34] E. Ott and J. C. Sommerer, Physics Letters A **188**, 39-47 (1994).

[35] J. C. Sommerer and E. Ott, Nature **365**, 138-140 (1993).

[36] J.F. Heagy, L.M. Pecora, and T.L. Carroll, Physical Review Letters **74** (21), 4185 (1994).

[37] S. Watanabe, H.S.J. van der Zant, S.H. Strogatz *et al.*, Physica D **97**, 429-470 (1996).

[38] G. Goldsztein and S.H. Strogatz, International Journal of Bifurcations and Chaos **5** (4), 983-990 (1995).

[39] J. Heagy , private communication.

[40] C.W. Wu and L.O. Chua, IEEE Transactions on Circuits and Systems - I **43** (2), 161-165 (1996).

[41] O.E. Rössler, Physics Letters **57 A**, 397 (1976).

[42] A.V. Oppenheim, G.W. Wornell, S.H. Isabelle *et al.*, *ICASSP-92 Proceedings*, San Francisco, 1992, **5**,IV-117-120 (IEEE,Piscataway, NJ)

[43] D.E. Rutherford, Proceedings of the Royal Society of Edinburgh **62**, 229 (1947).

[44] D.E. Rutherford, Proceedings of the Royal Society of Edinburgh **63**, 232 (1950).

[45] N.W. Aschroft and N.D. Mermin, *Solid State Physics* (Holt, Rinehart, and Winston, New York, NY, 1976).

[46] M. Golubitsky and D. Shaeffer, *Singularities and Groups in Bifurcation Theory, vol. I* (Springer-Verlag, New York, 1988).

[47] D. Armbruster and G. Dangelmayr, Math. Proc. Camb. Phil. Soc. **101**, 167 (1987).

[48] Tomasz Kapitaniak, International Journal of Bifurcations and Chaos **6** (1), 211 (1996).

[49] L. Kocarev and U. Parlitz, Physical Review Letters **76**, 1816 - 1819 (1996).

[50] C.W. Wu and L.O. Chua, IEEE Transactions on Circuits and Systems **42** (8), 430 (1995).

[51] R. Brown, CHAOS **7**, 395 (1996).

[52] M. di Bernardo, International Journal of Bifurcations and Chaos **6** (3), 557-568 (1996).

[53] W.L. Brogan, *Modern Control Theory* (Prentice Hall, Englewood Cliffs, NJ, 1991).

[54] M. Ding, W. Yang, V. In *et al.*, Physical Review **E 53** (5), 4334 (1996).

[55] G. Chen and X. Dong, International Journal of Bifurcations and Chaos **3**, 1363-1409 (1993).

[56] K. Pyragas, Physics Letters A **170**, 421 (1992).

[57] K. Pyragas, Physics Letters A **181**, 203 (1993).

[58] Paul So, Edward Ott, and W.P. Dayawansa, Physics Letters **A 176**, 421 (1993).

[59] L.M. Pecora and T.L. Carroll, Physical Review Letters **64**, 821 (1990).

[60] L.M. Pecora and T.L. Carroll, Physical Review **A 44**, 2374 (1991).

[61] T.L. Carroll and L.M. Pecora, IEEE Trans. CAS. **38**, 453 (1991).

[62] T.L. Carroll and L.M. Pecora, Physica **D 67**, 126-140 (1993).

[63] A. Turing, Philosophical Transactions **B 237**, 37 (1952).

[64] M. Golubisky, I.N. Stewart, and D.G. Schaeffer, *Singularities and Groups in Bifurcation Theory, vol. II* (Springer-Verlag, Berlin, 1988).

[65] F.A. Cotton, *Chemical Applications of Group Theory* (John Wiley and Sons, Inc, New York, 1971).

[66] B.E. Sagan, *The Symmetric Group* (Wadsworth & Brooks/Cole, Pacific Grove, CA, 1991).

[67] M. Tinkham, *Group Theory and Quantum Mechanics* (McGraw-Hill, New York, 1964).

[68] M. Hammermesh, *Group Theory and Its Application to Physical Problems* (Addison-Wesley, Reading, MA, 1962).

[69] P.C. Matthews and S.H. Strogatz, Physical Review Letters **65**, 1701 (1990).

[70] S. Nichols and K. Wiesenfeld, Physical Review **A 45**, 8430 (1992).

[71] D.G. Aronson, Martin Golubitsky, and J. Mallet-Paret, Nonlinearity **4**, 903-910 (1991).

[72] A.H. MacDonald and M. Plischke, Physical Review **B 27** (1), 201 (1983).

[73] T. Matsumoto, L.O. Chua, and M. Komuro, IEEE Transactions Circuits and Systems **32**, 797-818 (1985).

[74] T. Matsumoto, L.O. Chua, and K. Ayaki, IEEE Transactions Circuits and Systems **35**, 909-925 (1988).

[75] J.J. Torres, P.L. Garrido, and J. Marro, Journal of Physics **A 30** (22), 7801 (1997).

[76] S. Uchiyama and H. Fujisaka, Physical Review **E 56** (1), 99 (1997).

[77] J.K. John and R.E. Amritkar, Physical Review **E 51** (5), 5103 (1995).

[78] M. Mezard, G. Parisi, and M.A. Virasoro, *Spin Glass Theory and Beyond* (World Scientific, Singapore, 1987).

[79] L.M. Pecora, T.L. Carroll, G. Johnson *et al*., Physical Review Letters (to appear).